Viscoelastic Properties of Living Embryonic Tissues: a Quantitative Study

Gabor Forgacs,* Ramsey A. Foty,# Yinon Shafrir,§ and Malcolm S. Steinberg#

*Department of Physics and Biology, Clarkson University, Potsdam, New York 13699-5820 USA, #Department of Molecular Biology, Princeton University, Princeton, New Jersey 08544 USA, and §Department of Physics, Clarkson University, Potsdam, New York 13699 USA

ABSTRACT A number of properties of certain living embryonic tissues can be explained by considering them as liquids. Tissue fragments left in a shaker bath round up to form spherical aggregates, as do liquid drops. When cells comprising two distinct embryonic tissues are mixed, typically a nucleation-like process takes place, and one tissue sorts out from the other. The equilibrium configurations at the end of such sorting out phenomena have been interpreted in terms of tissue surface tensions arising from the adhesive interactions between individual cells. In the present study we go beyond these equilibrium properties and study the viscoelastic behavior of a number of living embryonic tissues. Using a specifically designed apparatus, spherical cell aggregates are mechanically compressed and their viscoelastic response is followed. A generalized Kelvin model of viscoelasticity accurately describes the measured relaxation curves for each of the four tissues studied. Quantitative results are obtained for the characteristic relaxation times and elastic and viscous parameters. Our analysis demonstrates that the cell aggregates studied here, when subjected to mechanical deformations, relax as elastic materials on short time scales and as viscous liquids on long time scales.

INTRODUCTION

It has long been known that certain embryonic tissues mimic the behavior of viscous liquids (Steinberg and Poole, 1982). During embryonic morphogenesis it is common for one cell population to spread over the surface of another, just as coalescing droplets of immiscible liquids do. In suspension or on nonadhesive surfaces, various multicellular aggregates round up in the manner of liquid droplets. Cells of two distinct tissues randomly intermixed within such aggregates sort out into separate regions in the manner of dispersions of immiscible liquids. In order to display such behavior, a system must 1) be composed of many subunits that 2) cohere while 3) being mobile. In ordinary liquids the subunits are molecules and the mobility is thermal; in rearranging cell populations the subunits are living cells and the mobility is ameboid. The differences must be kept in mind, but the shared properties cause tissues whose cells are mobile to behave, in many respects, as liquids.

To account for the liquid-like behavior of cell populations that display it, Steinberg formulated the "differential adhesion hypothesis" (DAH; Steinberg, 1963, 1964, 1970, 1993). According to the DAH, this behavior of cell populations, like that of ordinary liquids, is due to their possession of surface and interfacial tensions generated by adhesive and cohesive interactions between the component subunits (molecules in the one case, cells in the other). Recent experimental results have demonstrated that 1) tissue surface tension is a well-defined intensive physical parameter that characterizes the equilibrium shape of certain multicellular aggregates (Foty et al., 1994) and 2) the measured values of these tensions account for the observed mutual envelopment behavior of the corresponding tissues (Foty et al., 1996). Computer simulations applying the principles of the DAH and using specific statistical mechanical models reproduce the equilibrium configurations that tissues attain in the course of sorting out experiments (Glazier and Graner, 1993; Mombach et al., 1995).

Surface tension is an equilibrium property. Even if differences in surface tension contribute to the driving force for movement during morphogenesis, by themselves they reveal little about the time course of such processes. The kinetics of cell sorting and tissue envelopment depend upon the dynamical properties of cell populations. Early experiments by Phillips and Steinberg (1978; Phillips et al., 1977) showed that embryonic cell aggregates behave like deformable solids during brief experimental manipulations, but like viscous liquids in long-term organ cultures; that is, they possess complex viscoelastic characteristics. This is not surprising considering that major components of individual cells themselves display viscoelastic properties. The viscoelastic moduli of the cytoplasm of various cells have been measured (Hiramoto, 1968, 1969; Valberg and Albertini, 1985; Sakanishi, 1988; Hochmuth et al., 1993; Ragsdale et al., 1997). Detailed experiments on the viscoelasticity of solutions of major cytoplasmic biopolymers like microtubules, actin microfilaments, and intermediate filaments have been used to suggest possible specialized roles for the different classes of filaments in vivo (Zaner and Valberg, 1989; Müller et al., 1991; Janmey, 1991; Tempel et al., 1996). Following the deformations of red blood cells, Engelhardt and Sackmann (1988) were able to deduce values for the shear elastic moduli and viscosities of erythrocyte plasma membranes.

Received for publication 30 April 1997 and in final form 9 February 1998.

Address reprint requests to Dr. Gabor Forgacs, Department of Physics and Biology, Clarkson University, Potsdam, NY 13699-5820. Tel.: 315-268-2347; Fax: 315-268-6670; E-mail: forgacs@polaris.clarkson.edu.

0006-3495/98/05/2227/08 $2.00

Despite the fact that much information exists on the viscoelastic properties of various cellular components (Janmey, 1991), relatively little effort has been devoted to rheological studies of living tissues (Fung, 1993). Gordon et al. (1972) estimated the viscosity of several embryonic chicken cell populations, but the applied method gave no information on viscoelasticity. Most of the standard methods for the measurement of viscoelastic moduli (Fung, 1993) can not be easily applied to living embryonic tissues because of the special conditions required for the maintenance of the latter.

In this study we present a technique using our parallel plate compression apparatus, which allows a detailed quantitative study of tissue rheology. The method has previously been used to measure the surface tensions of a number of embryonic tissues (Foty et al., 1996). The main purpose of this article is to demonstrate that the behavior of living tissues can be analyzed in terms of standard models of viscoelasticity, appropriately modified to incorporate the specific biological properties of these systems. The results of the present study provide additional evidence that a number of properties of embryonic tissues under appropriate conditions can indeed be interpreted by exploiting their liquid-like behaviors.

MATERIALS AND METHODS

Preparation of cell aggregates

Fertile white Leghorn chicken eggs (Avian Services Inc., Frenchtown, NJ) were incubated at 37°C and 95% humidity for 3.5–6 days, depending on the tissue required. Limb bud mesoderm was obtained from 3.5- to 3.75-day-old embryos, heart ventricles, and livers from 5-day-old embryos and neural retinas from 6-day-old embryos. Dissections and dissociations were performed according to previously published methods (Steinberg, 1970; Moyer and Steinberg, 1976; Heintzelman et al., 1978; Thomas and Steinberg, 1981; Foty et al., 1996). Dissociated tissues were mechanically dispersed by gentle pipetting in Dulbecco's minimal essential medium with Earle's salts containing 10% horse serum (HyClone, Logan, UT), 50 μg/ml DNase I (Boehringer Mannheim), and the following antibiotics: 70 μg/ml gentamycin, 50 μg/ml penicillin-streptomycin-neomycin, and 50 μg/ml kanamycin (Gibco, Grand Island, NY). Dispersed cells were washed once in the above solution and then centrifuged to pellet clumps. The supernatants containing single cell suspensions were adjusted to a concentration of 10^6 cells/ml, and 3 ml were transferred to 10-ml tissue culture flasks (Bellco Glass, Vineland, NJ). Flasks were placed in a water bath/shaker at 37°C with 5% CO_2 for 2–4 h at 120 rpm, whereupon 3–4 $\times$ 10^6 cells per tube were transferred to round bottom glass tubes 15 mm in diameter, centrifuged, and cultured until they formed a firm, thin pellet (usually 2–4 h, depending on tissue type). These thin pellets were then cut into fragments about 1 mm in diameter and incubated on a gyratory shaker at 120 rpm under 5% CO_2 at 37°C until fragments rounded up (1.5–2 days, depending on tissue type).

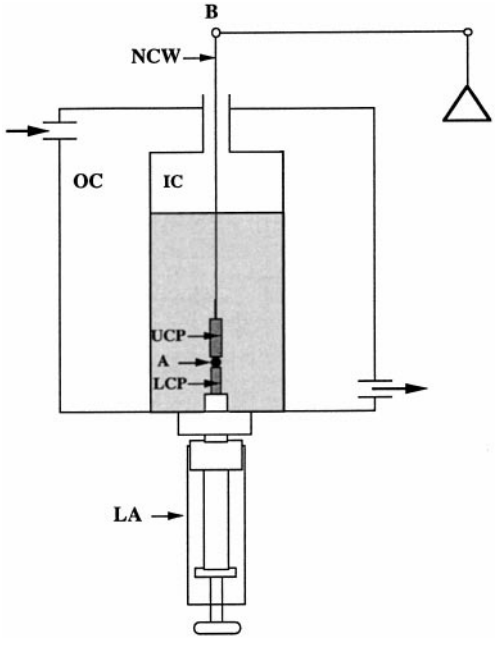

FIGURE 1 Schematic representation of the compression plate apparatus. Reprinted with permission from Foty et al., 1996.

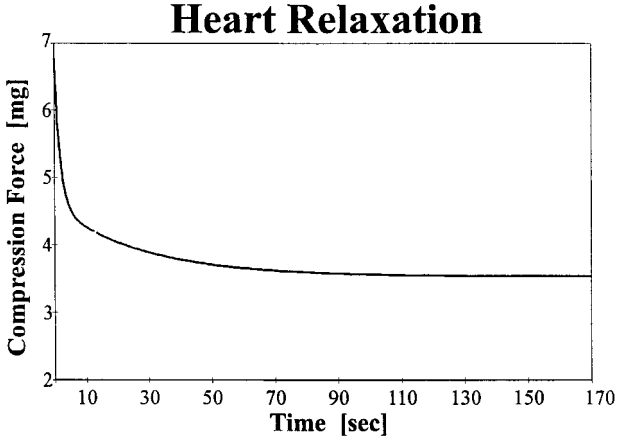

FIGURE 2 A characteristic compressive force relaxation curve (here shown for an embryonic heart aggregate).

Measurement of the viscoelastic response

The parallel plate compression apparatus used to measure the viscoelastic properties of living embryonic tissues is diagrammed in Fig. 1.

Previously used to measure tissue surface tensions, details of its operation and procedures followed in its use are described elsewhere (Foty et al., 1994, 1996). Multicellular aggregates of chicken embryonic cells (A), ranging in diameter from 200 to ~600 μm, were compressed between the parallel plates of this apparatus in sterile Eagle's minimal essential medium containing Hanks' balanced salt solution, 10% horse serum, and antibiotics (see above) at 37°C. An aggregate is positioned on the lower compression plate (LCP) in the inner chamber (IC). A circulating water bath maintains the temperature of water in the outer chamber (OC) at 37°C. Coating of the compression plates with poly(2-hydroxyethylmethacrylate) (Folkman and Moscona, 1978) minimizes the adherence of the aggregate to the plate. The upper compression plate (UCP) is suspended from the arm of a Cahn/Ventron (model 2000, Cerritos, CA) recording electrobalance (through a nickel-chromium wire, NCW). Recording of its apparent weight is used to establish a precompression zero force baseline. Raising the lower compression plate by turning the lower assembly (LA) compresses the aggregate between the two plates. A strip chart recorder continuously records changes in the force exerted by the aggregate upon the upper compression plate, equal to the changes in the apparent weight of the latter. In some cases aggregate profiles and times were continuously recorded at 25$\times$ magnification with a video cassette recorder connected to a video camera

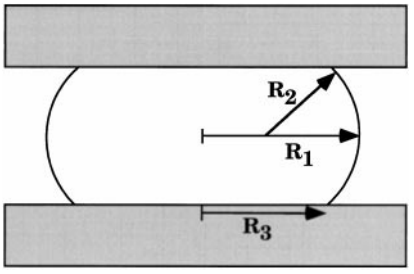

FIGURE 3 Definition of the quantities used in expression (1). R_1 and R_2 are the two principal radii of curvature at the droplet's equator and in a plane through the axis of symmetry. R_3 is the radius of the droplet's circular area of contact with the plates. Reprinted with permission from Foty et al., 1996.

coupled to a horizontal stereomicroscope. For experiments in which aggregate compression was intermittent, the positions of upper and lower compression plates were marked on the monitor screen to permit their accurate reproduction.

Measurement of cell size

Cell size was determined in cell suspensions by use of a calibrated stage micrometer and a compound microscope.

RESULTS

Tissue surface tension

The typical response of a living chicken embryonic multicellular aggregate to a sudden compression is shown in Fig. 2.

The chart recorder registers the time variation of the compressive force. In the present case it is the same as that of the initial compressive stress because the surface area to which the compression is applied does not change in the course of the relaxation process. The equilibrium value of the force, F_{eq}, defines the tissue surface tension σ through Laplace's equation

$$\frac{F_{eq}}{\pi R_3^2} = \sigma\left(\frac{1}{R_1} + \frac{1}{R_2}\right). \quad (1)$$

(In the conventional terminology applied to ordinary liquids in air, surface tension refers to the air-liquid interface and interfacial tension refers to an interface between two immiscible liquids. However, all measurements on living cell aggregates must be performed in tissue culture medium. We therefore use the term surface tension in reference to the aggregate-culture medium interface and reserve the term

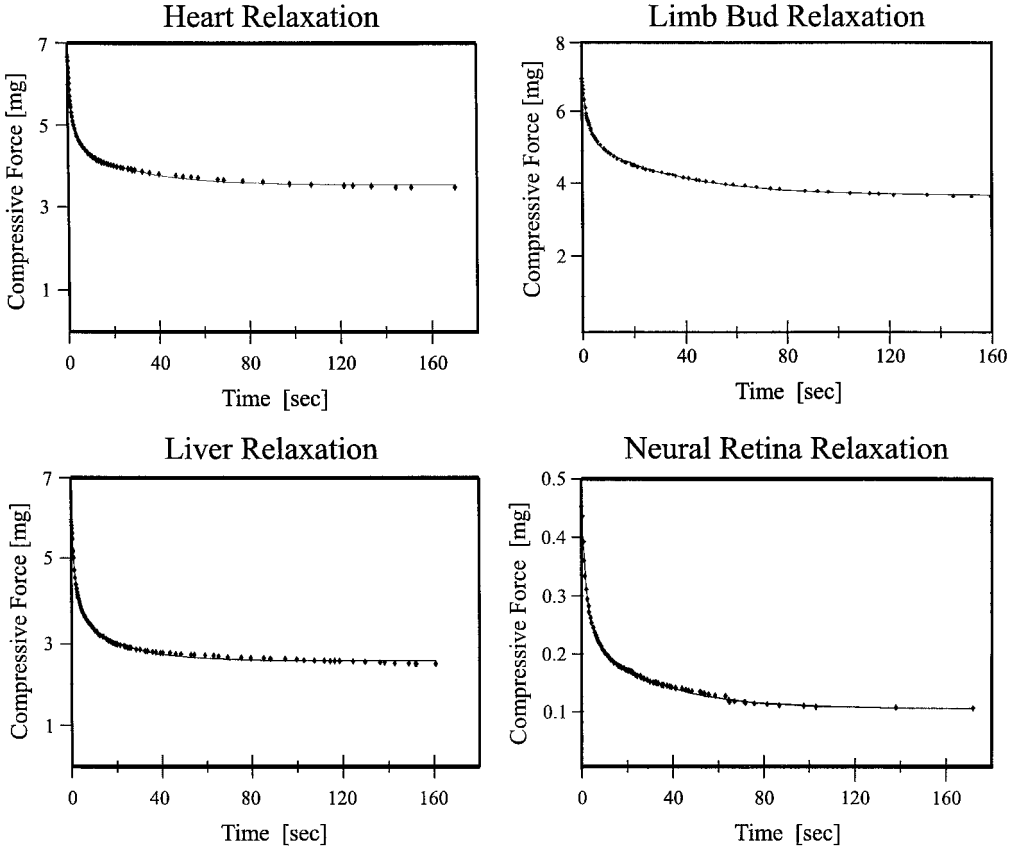

FIGURE 4 A representative relaxation process for each studied tissue. Dots denote experimental values along the measured relaxation curves, continuous lines are the best fits based on Eq. 7.

interfacial tension for reference to the interface between two different cell populations.) In Eq. 1, R_1 and R_2 are the principal radii of curvature as shown in Fig. 3 and πR_3^2 measures the area of contact between the cell aggregate and either of the parallel compression plates (Fig. 3).

Force relaxation

Relaxation curves similar to the one shown in Fig. 2 were obtained for multicellular aggregates derived from four embryonic chicken tissues: neural retina, liver, heart ventricle, and limb bud mesoderm (Fig. 4).

Full equilibration may take from less than 30 min to several hours, depending on the tissue. Because spheroidal cell aggregates subjected to a very brief compression spring back almost to their original shapes when released, whereas aggregates compressed for a longer time do not (Foty et al., 1996), such aggregates must be characterized as viscoelastic bodies. To distinguish the viscous from the elastic component of aggregate relaxation under compression, spheroidal aggregates of 5-day-old chick embryonic liver cells were subjected to a compressive force that was briefly interrupted at intervals during the approach to shape equilibrium. When compression was interrupted early in this process, the aggregate could be observed to considerably expand in height over the course of a few seconds. After this (mainly elastic) relaxation was complete (an ample 11 s were allowed for this), the compression plates were returned to their original positions and compression was resumed. This process was reiterated until the upper and lower surfaces of the aggregate remained planar after subsequent releases from compression, signifying the attainment of shape equilibrium. Aggregate profiles and times were continuously video recorded throughout each of these events. Aggregate heights and widths were measured for the transiently relaxed aggregate at the end of each interval of decompression. The height/width ratio of one such aggregate is plotted against cumulative time under compression in Fig. 5.

These measurements address changes in aggregate shape and demonstrate the rather clear separation of the viscous liquid and elastic components of the relaxation process. Results shown in Figs. 2 and 4, on the other hand, correspond to uninterrupted force relaxation and show the combined viscous liquid and elastic effects. Comparison of Fig. 5 with Fig. 4 (lower left) indicates that the very rapid relaxation observed in the first few seconds after initiation of compression of a liver aggregate largely reflects the elastic properties of the aggregate, comparable relaxation due to viscous liquid flow requiring several minutes. (Note that the curves in Figs. 4 and 5 correspond to slightly different relaxation phenomena and therefore should not necessarily be describable by the same analytic expression.)

The relaxation process is analyzed in terms of a generalized Kelvin-body model of viscoelasticity shown in Fig. 6.

The use of two dashpots (with friction constants μ_1 and μ_2) and two springs (with spring constants k_1 and k_2) is the simplest way to implement the bimodal process illustrated in Fig. 4. The system must possess at least two distinct relaxation times: a shorter one corresponding to the more elastic phase and a longer one corresponding to the more viscous phase. In general, biomaterials have a spectrum of relaxation times (Fung, 1993), but as will be shown below, all of our experimental curves can be reproduced very accurately with only two relaxation times. As discussed earlier, the equilibrium shape of the aggregate is determined by its surface tension, as modeled by the slidewire element (with surface tension σ) in Fig. 6.

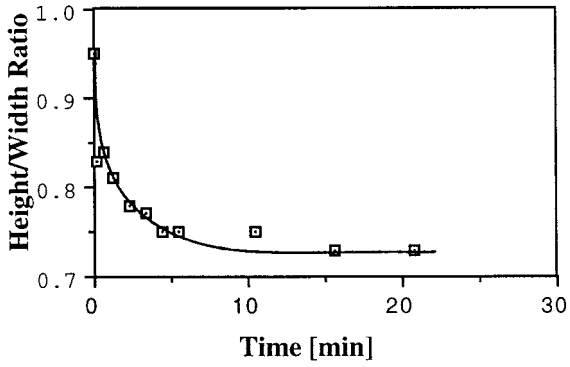

FIGURE 5 Liquid component of liver aggregate relaxation. An almost spherical chick embryonic liver aggregate was compressed under culture conditions between the parallel plates at a fixed separation distance and its profile shape video recorded. At intervals, the compression plates were separated for 11 s, allowing the aggregate to relax, after which compression was resumed. This process was reiterated until the upper and lower surfaces of the aggregate remained planar (shape equilibrium) after release from compression. **Squares** denote data points and the curve is drawn to lead the eye.

The force or stress relaxation can be summarized as follows. The initial sudden compression produces an instantaneous deformation of the slidewire element, u_0, and of the two springs, u_1 and u_2, whereas the initial displacement of the dashpots ($s_1(0)$ and $s_2(0)$) is zero. Consequently (see Fig. 6),

$$u_0(0) = u_1(0) = u_2(0), \quad s_1(0) = s_2(0) = 0. \tag{2}$$

The forces acting on the individual elements are given by

$$\begin{aligned} F_{S1}(t) &= k_1 u_1(t) = F_{D1}(t) = \mu_1 \dot{s}_1(t), \\ F_{S2}(t) &= k_2 u_2(t) = F_{D2}(t) = \mu_2 \dot{s}_2(t), \\ F_W(t) &= \sigma u_0(t) \end{aligned} \tag{3}$$

Here dots denote differentiation with respect to time and $F_{S1,2}$, $F_{D1,2}$, and F_W are the forces acting on the springs, dashpots, and slidewire element, respectively. The total deformation of the Kelvin-body and the corresponding force can be written as

$$\begin{aligned} u_t &= u_1 + s_1 = u_2 + s_2 = u_0, \\ F_t &= F_{S1} + F_{S2} + F_W = F_{D1} + F_{D2} + F_W \end{aligned} \tag{4}$$

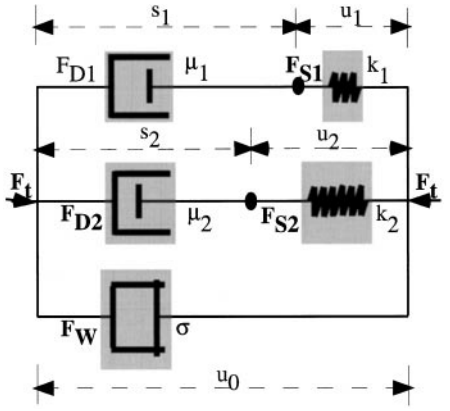

FIGURE 6 Illustration of the generalized Kelvin body used to model the relaxation process. All quantities are defined in the text.

The overall shape of the aggregate is practically unchanged during the force relaxation; therefore $u_t = u_0 = \text{const.}$, whereas the deformations of the springs decay while the dashpots gradually shrink. Finally, the equation governing the relaxation of F_t takes the form

$$F_t + \left(\frac{\mu_1}{k_1} + \frac{\mu_2}{k_2}\right)\dot{F}_t + \frac{\mu_1\mu_2}{k_1k_2}\ddot{F}_t = \sigma u_0. \quad (5)$$

In deriving Eq. 5, the relations given in Eq. 3 and Eq. 4 have been used. Equation 5 has to be solved with the initial condition (see Eq. 2)

$$F_t(0) = \sigma u_0 + k_1u_1(0) + k_2u_2(0) = (\sigma + k_1 + k_2)u_0. \quad (6)$$

The solution of Eq. 5 is then

$$F_t(t) = (\sigma + k_1e^{-t/\tau_1} + k_2e^{-t/\tau_2})u_0. \quad (7)$$

Here the two relaxation times are given by

$$\tau_i = \frac{\mu_i}{k_i}, \quad i = 1, 2. \quad (8)$$

As mentioned, at equilibrium all the stress is concentrated in the interfacial region. The solution of Eq. 5 leads to

$$u_i(t) = \frac{\mu_i}{k_i}\dot{s}_i(t) = e^{-t/\tau_i}u_0, \quad i = 1, 2. \quad (9)$$

which implies that in the limit of large t, indeed, the only force which differs from zero is F_w.

Data analysis

The relaxation curves obtained for the various embryonic tissues were fit to the expression given in Eq. 7. More specifically, the equilibrium value of the force, F_{eq} was obtained from the experimental curves. From Eq. 7, $F_{eq} = \sigma u_0$. This relationship defines u_0. (Comparison with Eq. 1 shows that u_0 is related to the geometric properties of the aggregate.) The difference $F_t(t) - F_{eq}$ is fit to the sum of two exponentials to reproduce Eq. 7. Each curve then yields four parameters, $\tau_i = \mu_i/k_i$ and $A_i = k_iu_0$, $i = 1,2$. These are used together with the results obtained for the surface tensions, σ (Foty et al, 1996) and $u_0 = F_{eq}/\sigma$ to obtain the spring constants and friction constants.

At least six aggregates of various sizes were tested for each of the four tissues. The aggregates were subjected to varying initial loads. All of the R^2 values for these fits were equal to or above 0.98. A representative fit for each tissue is shown in Fig. 4. Results for the model parameters are summarized in Table 1. As can be seen from the table there is indeed a clear separation of time scales given by τ_1 and τ_2 The fact that $k_1 > k_2$ and $\mu_2 > \mu_1$ is consistent with the characterization of the early phase of the relaxation process as more elastic and the later phase as more viscous (Fig. 5). The tissues are listed in Table 1 in the sequence of increasing σ. We note here that within the standard errors given in Table 1, the values of k_1, k_2, μ_1, and μ_2 are not inconsistent with the increase of these quantities in the same sequence. The last two columns (η, G) contain the values of viscosities and shear elastic moduli, which are obtained from the other model parameters (see Discussion).

DISCUSSION

A major challenge for a study such as the one reported here is to relate the model parameters derived from the measurements to specific processes, molecules, or structures in the cell. We have made some progress toward these goals. It should be noted that the compression of a system of mutually adherent soft viscoelastic beads would display a relaxation curve similar to the one shown in Fig. 2. However, in that case the value of σ in Eq. 1 would depend on the initial load. It has been experimentally demonstrated (Foty et al., 1996) that σ, as derived from Eq. 1 for the different tissues examined in this study, indeed has the attributes of liquid surface tension. Within the accuracy of our measurements,

TABLE 1 Values of the various model parameters discussed in the text

Cell type	τ_1 second	τ_2 second	σ dyne/cm	k_1 dyne/cm	μ_1 dynesec/cm	k_2 dyne/cm	μ_2 dynesec/cm	η Poise	G dyne/cm^2
Neural retina	2.2 ± 0.3	26.6 ± 5.2	1.6 ± 0.1	3.4 ± 0.5	7.3 ± 1.0	2.1 ± 0.3	55.2 ± 9.5	$\sim 10^5$	$\sim 10^3$
Liver	1.9 ± 0.2	22.5 ± 6.3	4.6 ± 0.1	4.0 ± 0.6	7.6 ± 1.5	2.3 ± 0.4	49.6 ± 13	$\sim 10^5$	$\sim 10^3$
Heart	1.9 ± 0.1	25.8 ± 5.4	8.5 ± 0.2	5.1 ± 0.6	9.5 ± 1.2	2.5 ± 0.3	66.0 ± 17	$\sim 10^5$	$\sim 10^3$
Limb	2.7 ± 0.2	44.8 ± 7.8	20.1 ± 0.5	8.6 ± 1.3	23.5 ± 4.4	7.7 ± 2.6	341 ± 116	$\sim 10^6$	$\sim 10^4$

τ_1, k_1, μ_1 and τ_2, k_2, μ_2 denote, respectively, the relaxation times, spring, and friction constants characterizing the model's two relaxation processes. σ denotes surface tension, η denotes viscosity, and G can be interpreted as the shear modulus of the tissue.

its value is independent of both the magnitude of the compressive force and of the size of the aggregate. If Eq. 1 holds for embryonic tissues, it means that any internal stress created by the initial compression is dissipated by the time the system reaches equilibrium. Any stress that remains must reside in the surface layer or interface between the aggregate and the surrounding tissue culture medium. This is in accord with the time evolution of the shape of individual cells within the aggregate. Aggregates of both chick (Phillips et al., 1977) and amphibian (Phillips and Davis, 1978) embryonic cells have been fixed at various points on their way to equilibrium after application of a distorting stress and then sectioned to observe the shapes of the component cells. In each case, internal cells were initially stretched upon application of the distorting force but then gradually recovered their precompressed cuboidal shapes as the aggregates approached shape equilibrium. These observations are schematically illustrated in the bottom row of Fig. 7, which shows the early, more elastic response followed by a later, more viscous response.

The initial shape transformation of the cells requires work to be done against the cells' bending rigidity, elastic tension, and the resistance to deformation of any extracellular matrix that might be present. In order to proceed from the elastically deformed state to the final state shown at the bottom right in Fig. 7, cells have to slide along each others' surfaces and overcome the arising friction. The middle row in Fig. 7 shows the evolution of cell perimeters as traced from electron micrographic cross-sections of embryonic chick liver cell aggregates deformed by a continuous, 2000 $\times$ g centrifugation (Phillips et al., 1977) rather than by compression between parallel plates. Above each cross-section is shown the profile shape of the aggregate fixed during centrifugation from which it was taken. Equivalent cell shape changes have been documented in aggregates of frog gastrula internal endoderm cells compressed between parallel plates (Phillips and Davis, 1978). Thus, cells in liquid-like cell aggregates continuously subjected to a distorting stress initially display a strain that eventually is dissipated independently of the means by which the stress distorting the aggregate as a whole is applied. Similar studies are under way with compressed aggregates of cells genetically engineered to express different numbers of a given cell adhesion molecule.

In view of the bimodal relaxation process illustrated in Fig. 7, we interpret τ_1 as the time scale characterizing the relaxation of the more or less elastic deformation of each individual cell in the aggregate, together with whatever extracellular matrix molecules might be present. This elastic stress is quickly dissipated and is followed by a long viscous response (characterized by the much larger relaxation time τ_2) in the course of which individual cells move and the interior of the aggregate is reorganized. This motion requires that cells break and reform their adhesive contacts with their neighbors. Therefore, it is plausible to assume 1) that the greater the binding energy between adhesion molecules, the more stable these contacts will be and 2) that the friction experienced by the rearranging cells will be in direct relation to the number of adhesion molecules bridging their surfaces. A simple dimensional analysis of the friction constant describing the more viscous phase reveals that it can be written as $\mu_2 = cJN\tau$. Here J can be interpreted as the effective binding energy between cell adhesion molecules containing both their direct and indirect interactions, the latter being mediated by the cell's elastic tension and attachments to adjoining cytoskeletal and other molecules. τ is the characteristic lifetime of the adhesive contacts, N is the number of these contacts per unit area and c is a

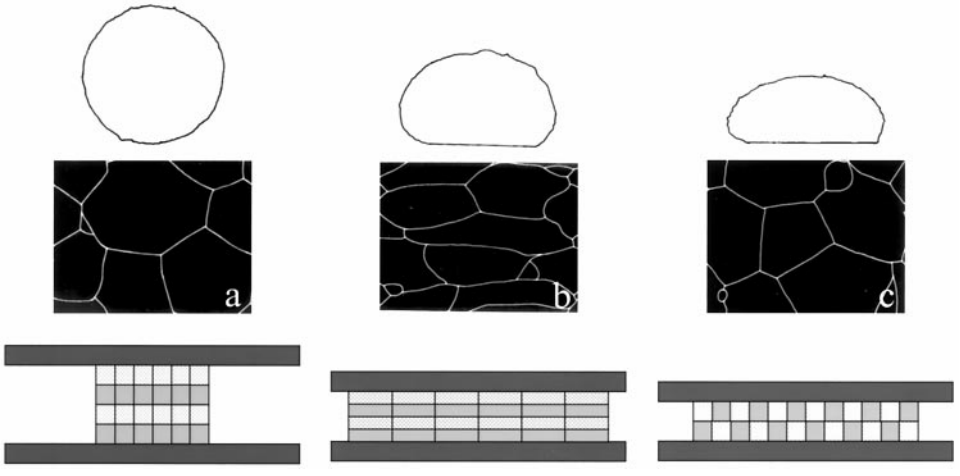

FIGURE 7 The bimodal relaxation process. *Bottom*: Schematic representation using cuboidal cells and aggregates. *Middle*: Cell perimeters traced from electron micrographic horizontal sections taken just below the widest point of the chick embryonic liver aggregates profiled above (Phillips et al., 1977). (*a*) Spherical aggregate before centrifugation, showing isodiametric cells. (*b*) Aggregate fixed under centrifugation at 2000 $\times$ g, applied for 5 min, showing internal cells under tension during the rapidly relaxing, more elastic phase. (*c*) Aggregate fixed under centrifugation at 2000 $\times$ g, applied for 36 hr, showing the final equilibrium state. Although the aggregate is much more flattened than at 5 min, the cells within it have fully relaxed and rearranged as diagrammed below.

dimensionless constant. If we assume, according to the DAH, that tissue surface tension is due to adhesive and cohesive interactions, a similar analysis leads to $\sigma = \hat{c}\,JN$, in which $\hat{c}$ is another constant. We are pursuing the evaluation of the relations $\mu_2 = c\,JN\,\tau$, $\sigma = \hat{c}\,JN$, and $\mu_2 \propto \sigma\tau$ (implied by the first two) through the use of cell populations genetically engineered to express adhesion molecules exclusively of a single kind in precisely regulated amounts. (Various members of the cadherin family of homophilic cell-cell adhesion molecules are known to be active in the tissues studied here, but no complete inventory exists of the adhesion molecules expressed by these or any other naturally occurring cell types, nor have adhesion molecules' binding energies, turnover times, etc. yet been reported.)

Our analysis of the data is based on a simple generalization of the Kelvin model commonly used to study the viscoelasticity of biological systems (Sakanishi, 1988; Fung, 1993). The Kelvin model deals with forces, displacements, and velocities. In a more sophisticated analysis, the basic relations between forces, displacements, and velocities given in Eq. 3 would be replaced with constitutive equations of the tissue relating the stress tensor to the deformation tensor and its time derivatives (Byrd et al., 1977). Experimental results would then yield values for viscosities (η) and shear moduli (G). The precise relationship between spring constants and friction constants used in this study and viscosities and shear moduli depends on the detailed microscopic dynamics of the system. (An example is the celebrated Stokes law, $F = 6\pi a\eta v$, giving the frictional force exerted by a Newtonian fluid of viscosity η on a spherical particle with radius a moving with uniform velocity v. To derive Stokes law, one has to solve the entire Navier-Stokes equation (Landau and Lifshitz, 1978), a formidable task in general.)

The middle row of Fig. 7 reveals that the studied cell aggregates resemble foams or concentrated emulsions (Prause et al., 1995). These latter systems are known to have complex, nonlinear viscoelastic behavior (Kraynik, 1988). The mathematical analysis of their rheological and elastic properties is so complicated (Princen and Kiss, 1989; Reinelt and Kraynik, 1990; Kraynik et al., 1991; Weaire et al., 1992; Pithia and Edwards, 1994) that it has been carried out mostly under simplifying assumptions (two dimensions, affine deformations, special geometry, etc.). Living tissues are considerably more complex than foams and concentrated emulsions. Because of this complexity our aim here is to use the simplest model that may adequately account for the experimental findings. The studied tissues were tested in a range of initial loads for which the linear Kelvin model (although representing a strong oversimplification) leads to a rather accurate description of our results. (We note that despite its simplicity, the Kelvin model has been used to model the rheology of foams (Pithia and Edwards, 1994)). Even if the linear analysis for the applied loads correctly reflects the response of the tissues, beyond a certain compression it is bound to break down and cells would be injured or destroyed.

Some information on tissue viscosity and shear elastic modulus can be obtained in the following way. F_{D2} in Eq. 4 is the dominant force exerted by the aggregate on either of the compression plates in the more viscous phase of the relaxation process. In terms of stresses, $F_{D2} = \sigma^0 A$, in which A is the droplet's circular area of contact with the plates and with σ^0 being the appropriate component of the stress tensor along the contact area, as illustrated in Fig. 3 (we assume here that σ^0 is constant along A). This force is the consequence of the displacement of the cells along the contact, and therefore σ^0 is a shear stress arising in the course of this motion. (s_2 in Eq. 3 is then interpreted as the total displacement of all the cells in the contact area.) Even if at this time the cell aggregate is considered as a Newtonian fluid, to obtain σ^0 one needs information on the flow field, which is not available to us. However, because the shear stress is caused by the friction between individual cells, it can be approximated as $\sigma^0 = \eta v/a$, with η, v, and a, respectively, being the viscosity of the tissue, the typical velocity, and the radius of a cell. Because A is proportional to Na^2 (with N being the number of cells in the contact area), using the relationship between F_{D2} and s_2 (with $\dot{s}_2 = Nv$) given in Eq. 3, leads to $\mu_2 = Ca\eta$. Here C is a constant. A similar analysis in the more elastic phase of the relaxation process would lead to $k_1 = CaG$, in which G can be interpreted as the shear modulus of the tissue. The size of cells before incorporation into the aggregates was measured as described earlier. Assuming then that C is of the order of unity, we finally obtain the estimates for η and G given in Table 1. The estimates for the viscosities are comparable with the results reported by Gordon et al. (1972).

The above analysis provides estimates of the viscoelastic moduli of cell aggregates derived from various tissues. We note that the results for the characteristic relaxation times are the same whether μ, k or η, G is used (Byrd et al., 1977) and, we believe, represent an accurate characterization of tissue viscoelasticity.

Viscoelastic properties of individual cells have been extensively studied in the past (Hiramoto, 1968, 1969; Valberg and Albertini, 1985; Luby-Phelps et al., 1986; Sakanishi, 1988; Hochmuth et al., 1993; Jay et al. 1993; Ragsdale et al., 1997). The reported results are diverse, revealing that these physical parameters strongly vary with cell type.

The present study deals with the viscoelastic properties of aggregates that consist of many thousands of cells. As mentioned, the ultimate goal of such study is to unravel the relationship between the tissue specific values of viscoelastic parameters and their cell specific counterparts and eventually relate these physical quantities to molecular components. In addition, the viscoelastic properties of multicellular aggregates deserve attention for they are important determinants of mechanical behavior, which differs greatly among such tissues as bone, tendon, lung, the walls of the uterus and urinary bladder, and the germ layers of early-stage embryos. The mechanical properties of these tissues range from those of a relatively inelastic solid

through a range of viscoelastic differences to those of a viscous liquid. Quantification of these properties is important for the understanding of the dynamics of morphogenetic processes and the biomechanics of tissue structures. It is also of practical importance for the design of implantable medical devices and of the biomaterials used in their fabrication.

Supported by research Grants IBN 97–10010 from the National Science Foundation (G. Forgacs) and GM52009 from the National Institute of General Medical Sciences (M. S. Steinberg).

REFERENCES

Byrd, B. R., R. C. Armstrong, and O. Hassager. 1977. Dynamics of Polymeric Liquids. John Wiley & Sons, New York.

Engelhardt, H., and E. Sackmann. 1988. On the measurement of shear elastic moduli and viscosities of erythrocyte plasma membranes by transient deformation in high frequency electric fields. *Biophys. J.* 54: 495–508.

Folkman, J., and A. Moscona. 1978. Role of cell shape in growth control. *Nature.* 273:345–349.

Foty, R. A., G. Forgacs, C. M. Pfleger, and M. S. Steinberg. 1994. Liquid properties of embryonic tissues: measurement of interfacial tensions. *Phys. Rev. Lett.* 72:2298–2301.

Foty, R. A., C. M. Pfleger, G. Forgacs, and M. S. Steinberg. 1996. Surface tensions of embryonic tissues predict their envelopment behavior. *Development.* 122:1611–1620.

Fung, Y. C. 1993. Biomechanics. Springer-Verlag, New York.

Glazier, J. A., and F. Graner. 1993. Simulation of the differential adhesion driven rearrangement of biological cells. *Phys. Rev.* E47:2128–2154.

Gordon, R., N. S. Goel, M. S. Steinberg, and L. L. Wiseman. 1972. A rheological mechanism sufficient to explain the kinetics of cell sorting. *J. Theor. Biol.* 37:43–73.

Heintzelman, K. F., H. M. Phillips, and G. S. Davis. 1978. Liquid-tissue behavior and differential cohesiveness during chick limb budding. *J. Embryol. Exp. Morphol.* 47:1–15.

Hiramoto, Y. 1968. Observation and measurements of sea urchin eggs with a centrifuge microscope. *J. Cell Physiol.* 69:219–230.

Hiramoto, Y. 1969. Mechanical properties of the protoplasm of the sea urchin egg. *Exp. Cell Res.* 56:201–208.

Hochmuth, R. M., H. P. Ting-Beal, B. B. Beaty, D. Needham, and R. Tran-Son-Tay. 1993. Viscosity of passive human neutrophils undergoing small deformations. *Biophys. J.* 64:1596–1601.

Janmey, P. A. 1991. Mechanical properties of cytoskeletal polymers. *Curr. Opin. Cell Biol.* 2:4–11.

Jay, P. Y., C. Pasternak, and E. L. Elson. 1993. Studies of aspects of amoeboid locomotion. *Blood Cells.* 19:375–386.

Kraynik, A. M. 1988. Foam flows. *Annu. Rev. Fluid. Mech.* 20:325–357.

Kraynik, A. M., D. A. Reinelt, and H. M. Princen. 1991. The nonlinear elastic behavior of polydisperse hexagonal foams and concentrated emulsions. *J. Rheology.* 35:1235–1253.

Landau, L. D., and E. M. Lifshitz. 1978. Fluid Mechanics. Pergamon Press, New York.

Luby-Phelps, K., D. L. Taylor, and F. Lanni. 1986. Probing the structure of the cytoplasm. *J. Cell Biol.* 102:2015–2022.

Mombach, J. C. M., J. A. Glazier, R. C. Raphael, and M. Zajac. 1995. Quantitative comparison between differential adhesion models and cell sorting in the presence and absence of fluctuations. *Phys. Rev. Lett.* 75:2244–2247.

Moyer, W. A., and M. S. Steinberg. 1976. Do rates of intercellular adhesion measure the cell affinities reflected in cell-sorting and tissue spreading configurations? *Dev. Biol.* 52:246–262.

Müller, O., H. E. Gaub, M. Bärmann, and E. Sackmann. 1991. Viscoelastic moduli of sterically and chemically cross-linked actin networks in dilute to semidilute regime: measurements by an oscillating disc rheometer. *Macromolecules.* 24:3111–3120.

Phillips, H. M., and G. S. Davis. 1978. Liquid-tissue mechanics in amphibian gastrulation: germ-layer assembly in *Rana pipiens. Am. Zool.* 18:81–93.

Phillips, H. M., and M. S. Steinberg. 1978. Embryonic tissues as elasticoviscous liquids: I. Rapid and slow shape changes in centrifuged cell aggregates. *J. Cell Sci.* 30:1–20.

Phillips, H. M., M. S. Steinberg, and B. H. Lipton. 1977. Embryonic tissues as elasticoviscous liquids: II. Direct morphological evidence for cell slippage in centrifuged aggregates. *Dev. Biol.* 59:124–134.

Pithia, K. D., and S. F. Edwards. 1994. Rheology of liquid foams. *Physica.* A205:565–576.

Prause, B. A., J. A. Glazier, S. J. Gravina, and C. D. Montemagno. 1995. Three dimensional magnetic resonance imaging of a liquid foam. *J. Phys. Cond. Matt.* 7:L511–L516.

Princen, H. M., and A. D. Kiss. 1989. Rheology of foams and highly concentrated emulsions: IV. An experimental study of the shear viscosity and yield stress of concentrated emulsions. *J. Colloid Interface Sci.* 128:176–187.

Ragsdale, G. K., J. Phelps, and K. Luby-Phelps. 1997. Viscoelastic response of fibroblasts to tension transmitted through adherens junctions. *Biophys. J.* 73:2798–2808.

Reinelt, D. A., and A. M. Kraynik. 1990. On the shearing flow of foams and concentrated emulsions. *J. Fluid. Mech.* 215:431–455.

Sakanishi, T. Y. 1988. Effects of viscoelasticity of cytoplasm on the complex viscosity of red blood cell suspensions. *Biorheology.* 25: 123–128.

Steinberg, M. S. 1963. Reconstruction of tissues by dissociated cells. *Science.* 141:401–408.

Steinberg, M. S. 1964. The problem of adhesive selectivity in cellular interactions. *In* Cellular Membranes in Development. M. Locke, editor. Academic Press, New York. 321–366.

Steinberg, M. S. 1970. Does differential adhesion govern self-assembly processes in histogenesis? Equilibrium configurations and the emergence of a hierarchy among populations of embryonic cells. *J. Exp. Zool.* 173:395–434.

Steinberg, M. S. 1993. The assembly of embryonic cells into tissues and organs mimics liquid behavior and is guided by interfacial energies arising from cellular adhesive interactions. *In* Dynamical Phenomena at Interfaces, Surfaces and Membranes. D. Beysens, N. Boccara, and G. Forgacs, editors. Nova Science Publishers, Commack, New York. 3–10.

Steinberg, M. S., and T. J. Poole. 1982. Liquid behavior of embryonic tissues. *In* Cell Behaviour. R. Bellairs, A. S. G. Curtis, and G. Dunn, editors. Cambridge University Press, Cambridge. 583–607.

Tempel, M., G. Isenberg, and E. Sackmann. 1996. Temperature-induced sol-gel transition and microgel formation in α-actinin cross-linked actin networks: a rheological study. *Phys. Rev.* E54:1802–1810.

Thomas, W. A., and M. S. Steinberg. 1981. Two distinct adhesion mechanisms in embryonic neural retina cells: I. A kinetic analysis. *Dev. Biol.* 81:96–105.

Valberg, P. A., and D. F. Albertini. 1985. Cytoplasmic motions, rheology and structure probed by a novel magnetic particle method. *J. Cell Biol.* 101:130–140.

Weaire, D., F. Bolton, and T. Herdtle. 1992. The effect of strain upon the topology of soap froth. *Phil. Mag. Lett.* 66:293–299.

Zaner, K. S., and P. A. Valberg. 1989. Viscoelasticity of F-actin measured with magnetic microparticles. *J. Cell. Biol.* 109:2233–2243.